Hindawi
Advances in Civil Engineering
Volume 2024, Article ID 5564418, 13 pages
https://doi.org/10.1155/2024/5564418

Research Article

Model Test Study of Rainfall Factors on Failure Process of Xiashu Loess Slope with Gravel Layer

Yanran Hu [1,2] **Shaorui Sun** [1] **and Yuyong Sun** [2]

[1]School of Earth Sciences and Engineering, Hohai University, Nanjing 211111, China
[2]School of Architectural Engineering, Tongling University, Tongling 244000, China

Correspondence should be addressed to Shaorui Sun; ssrfish@hhu.edu.cn

Received 3 August 2023; Revised 19 December 2023; Accepted 21 December 2023; Published 16 January 2024

Academic Editor: Hailing Kong

Rainfall is an important factor affecting the stability of Xiashu loess slope, so it is particularly important to understand the infiltration law and induction process of rainfall in Xiashu loess slope. In this paper, a Xiashu loess slope model with a slope ratio of 1 : 1.2 is constructed in the model box. The rainfall infiltration law, vertical stress characteristics, pore-water pressure characteristics, and deformation failure mode of the slope under two different rainfall types and four different rainfall degrees are analyzed. The instability and failure mechanism of Xiashu loess slope with gravel layer under different rainfall conditions is studied. The test results show that the influence of rainfall intensity factors on the gravel soil slope is mainly reflected in the degree of erosion of the slope. With the increase in rainfall frequency and intensity, the rainfall infiltration rate gradually increased, reached the highest value after standing, and then decreased with the increase of rainfall intensity. Rainfall has a great influence on the pore-water pressure in the gravel soil slope, and the pore-water pressure at the monitoring point of the slope toe changes the most. The vertical stress curve will change abruptly in the later stage of intermittent rainfall and during continuous rainfall.

1. Introduction

Xiashu loess is a special kind of eolian soil distributed in China. It was formed in the late Pleistocene of Quaternary and widely developed in the middle and lower reaches of the Yangtze River [1, 2]. Xiashu loess is sensitive to water, and its physical and mechanical properties are significantly different under dry and wet conditions [3–6]. The development of vertical joints in Xiashu loess slope provides conditions for rainfall infiltration, which is prone to slope instability [7, 8]. Xiashu loess landslide has become one of the most common geological disasters that hinder economic and social development in low mountain and hilly areas such as Ningzhen, Yili, Suzhou, Wuxi, and Changzhou [9–11] due to its high risk and difficulty in prediction. Therefore, it is of great theoretical and practical engineering significance to study the influence of rainfall factors on the stability of Xiashu soil slope.

The research on the influence of rainfall on the stability of soil slopes is relatively mature. Similar to the analysis and prediction of cavern stability [12, 13], monitoring the influence of specific factors is an effective means to study slope. Okura et al. [14], Rahardjo et al. [15], Damiano and Olivares [16], and other foreign scholars monitored and analyzed the changes in pore-water pressure of actual soil slopes during rainfall. It is found that the increase of pore-water pressure is the main factor leading to slope instability. Guo et al. [17] obtained the rainfall response characteristics, time characteristics, and temporal and spatial variation of rainfall infiltration of the slope by monitoring a landslide hazard point on the southeast coast for half a year. Combined with the previous experience, a slope rainfall infiltration model considering the uneven distribution of initial water content was established [18–20]. Therefore, with the gradual improvement of the similarity scale principle, the indoor model test has been more widely used because of its low cost, controllable boundary conditions, and easy operation. The rainfall slope model test can intuitively show the failure process of the slope, and can timely find the changes of various parameters in the process of rainfall infiltration [21, 22]. This is an important means to study the mechanism of slope instability. Indoor model tests include ordinary 1 g model, full-scale model, and centrifugal model tests [23, 24]. Because the latter two are

Table 1: Particle size distribution.

Size (mm)	<0.002	0.002–0.005	0.005–0.075	>0.075
Percent (%)	1.14	72.45	6.55	19.86

Table 2: Physical parameters of Xiashu loess.

G_S	Liquid limit (%)	Plastic limit (%)	Free swelling ratio (%)	Optimum water (%)
2.73	30.01	15.47	48.85	16.14

limited by many conditions, the ordinary 1 g model is often used for research. Hu et al. [25] carried out a series of indoor tests on the instability of granite residual soil slopes with slope gradient and rainfall intensity as variables and combined with computer image processing technology to obtain the microscopic slip law of the slope. Zeng et al. [26] established an indoor scale model with a loess slope in Qingyang, Gansu Province as the research object. By analyzing the changes in slope volumetric water content and matric suction during the experiment, they found the difference in the infiltration law of the slope model under different rainfall intensities. To overcome the problem that the slope strain is difficult to monitor, Zhu et al. [27] used Brillouin time domain analysis technology to continuously monitor the strain of soil at different depths in the slope model during the loading process of the slope top and found that the maximum value of the average strain in the horizontal direction will affect the stability of the slope. Chueasamat et al. [28] studied the influence of surface sand density and rainfall intensity on slope failure based on the 1g slope model, and found that the slope failure mechanism was surface slide failure and retrogressive. Based on the indoor slope model, Take et al. [29] analyzed the potential triggering mechanism of the rapid landslide of the fill slope. Tohari et al. [30] clarified the instability and sliding process of the soil slope based on the laboratory-scale soil slope model test, and found that the slope failure began from the toe of the slope. Gallage et al. [31] studied the influence of slope inclination on slope stability, and found that when the slope inclination is greater than 1.2 times the soil friction angle, the failure is caused by the loss of soil suction. On the contrary, the failure is caused by the positive pore pressure. Orense et al. [32] monitored the pore-water pressure, soil moisture content, and slope surface displacement on the sandy slope model, and determined the process of slope failure induced by rainfall.

In summary, the researchers used field tests, indoor model tests, and numerical simulations to study the stability of soil slopes. There are relatively few studies on the soil slope with gravel layer by means of an indoor model test. In this paper, the model of the soil slope with a gravel layer is constructed in the model box, and the self-made artificial rainfall device is used to simulate the natural rainfall. From the aspects of rainfall infiltration law, vertical stress characteristics, pore-water pressure characteristics, and deformation failure mode of the slope, the failure mechanism of the soil slope with gravel layer under different rainfall conditions are discussed.

2. Model Test Design

2.1. Physical Properties of Test Soil Samples. Xiashu loess was collected from the slope near Huwu Expressway in Jurong City, Zhenjiang City, Jiangsu Province. The soil samples were grayish–yellow–brown. To understand the basic physical and mechanical properties of soil samples, indoor geotechnical tests were carried out. The results are shown in Tables 1 and 2.

2.2. Experimental Device. The indoor model experimental device used in the study mainly includes a model box, an artificial rainfall system, a monitoring system, and an acquisition system. Figures 1 and 2 are the main experimental device and model diagram.

(1) Limited by the test site, the size of the model box was designed as 2.4 m × 1 m × 0.9 m (length × width × height). To restrain the lateral deformation of the slope during the test, transparent acrylic plates were used as side baffles on both sides of the model box, as shown in Figure 1(b).

(2) The artificial rainfall device was consisted of an atomizing nozzle and a polyvinyl chloride (PVC) hose, as shown in Figures 1(a) and 1(b). The rainfall system had four pipelines. Four atomizing nozzles were distributed on each line, which relates to PVC hose by means of flat tee. The outlet of atomizing nozzle is water mist, and the flowmeter is installed at the inlet as shown in Figure 1(c). A single nozzle can be closed and the flow rate can be adjusted. The intensity and uniformity of rainfall can be controlled by controlling the opening and closing of atomizing nozzles at different positions and the flow rate. The spraying flow rate is 0–0.8 L/hr, and the spraying diameter is about 1 m. It can meet the test requirements.

(3) DMKY pore-water pressure gauge was used to monitor the change of pore-water pressure during rainfall. The TZT-MT earth pressure gauge was used to monitor the vertical stress changes, as shown in Figures 1(d) and 1(f). The two trisection planes of the slope along the strike direction were used as the slope of the sensor. Three pore-water pressure gauges and three soil–pressure gauges are arranged at the top, middle, and bottom of the slope, respectively, as shown in Figure 1. The pore-water pressure gauges and soil–pressure gauges at the foot, middle, and top

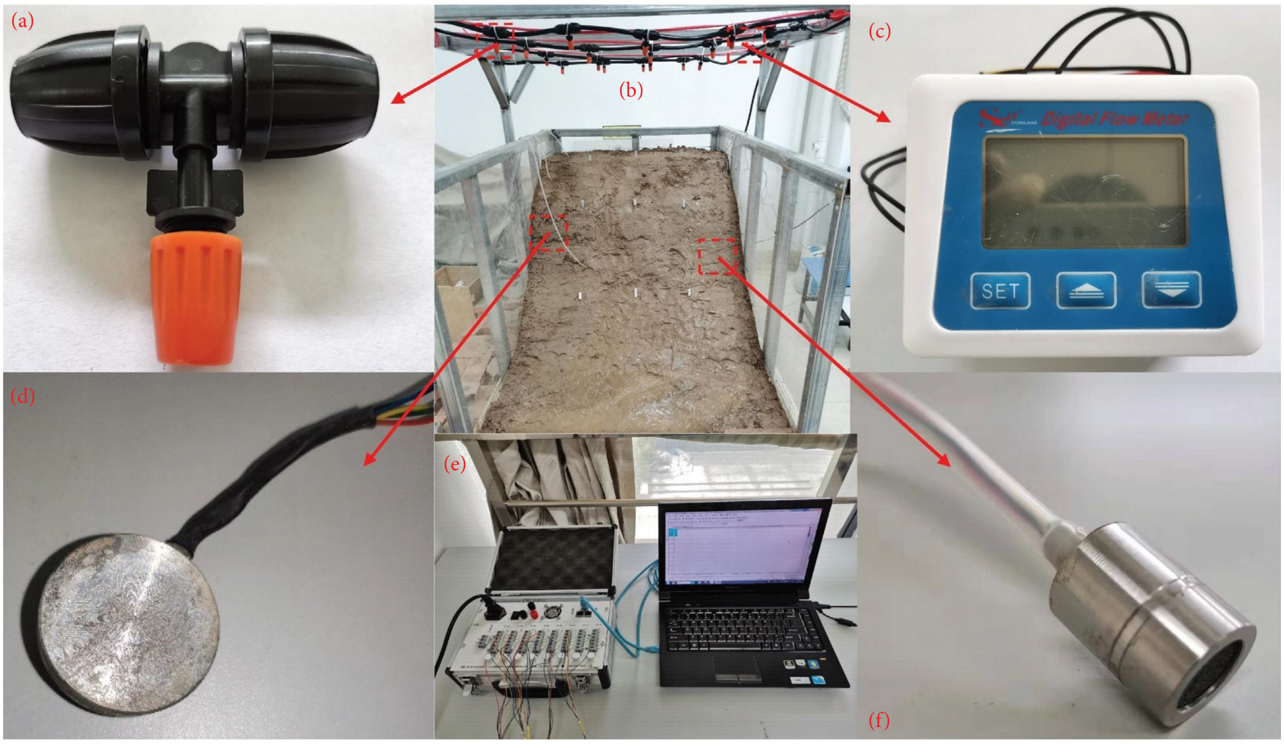

Figure 1: Monitoring instruments: (a) adjustable atomizing nozzle, (b) artificial rainfall system, (c) flowmeter, (d) soil–pressure gauge, (e) signal acquisition instrument, and (f) pore water-pressure gauge.

of the slope are named K1, K2, K3 and T1, T2, T3, respectively, as shown in Figure 2.

The deformation monitoring of the slope was carried out by embedding 15 cm × 1 cm (length × width) wood chips on its surface as an observation support. A reflector was pasted on the top of the bracket. The total station could be used to monitor the change in slope displacement. To fully observe the slope deformation, three monitoring lines were laid along the slope direction. They were located at the top, middle, and foot of the slope. There were three displacement monitoring points on each monitoring line, a total of nine monitoring points, numbered W1–W9, as shown in Figure 2(c). The monitoring content is the horizontal displacement and vertical displacement of the slope table. The monitoring frequency was measured once every 30 min. When the slope is found to be obviously damaged, the number of monitoring should be appropriately increased.

(4) The data acquisition system is TST3827E dynamic and static signal acquisition instrument, as shown in Figure 1(e). There are eight channels in the instrument. It can realize signal synchronous sampling, synchronous transmission, real-time display, and real-time storage. Slope pore-water pressure and vertical stress can also be collected at the same time.

2.3. Experimental Process. The study area is a north subtropical monsoon climate with four distinct seasons, abundant heat, and abundant rainfall. According to the meteorological department, the rainfall in this area is mainly concentrated from June to July. The related disastrous weather is mainly manifested as rainstorms and short-duration heavy precipitation. The maximum hourly rainfall intensity in the past 2 years is as high as 88.0 mm/hr. This experiment simulated four different rainfall intensities of 20, 50, 70, and 90 mm/hr. The influence of different rainfall types, different rainfall intensities, and different rainfall times on the stability of the Xiashu loess slope is studied. The intermittent rainfall is divided into four times, each rainfall is 180 min, and the interval between two adjacent rainfalls is 2 days. After the intermittent rainfall, to restore the initial state of the seepage field in the slope, the continuous rainfall started after 4 days of standing. The continuous rainfall is also divided into four times, but there is no interval between the two rainfall intensities. The whole rainfall process lasted from the beginning of the experiment to the end of the experiment. The rainfall arrangement is shown in Figure 3.

The top and bottom of the test slope model are Xiashu loess, and there is a certain thickness of gravel layer in the middle. The profile is shown in Figure 2(b).

(1) The slope model uses the wooden board as the base to simulate the underlying bedrock, and the slope rate is 1 : 1.2 (as shown in Figure 2(c)). The ratio design of the slope is based on an actual slope case from Jiangsu Province, China. A grid line with an interval of 10 cm is drawn on the side acrylic baffle to observe rainwater infiltration and slope damage. Vaseline was evenly applied to the inner wall of the

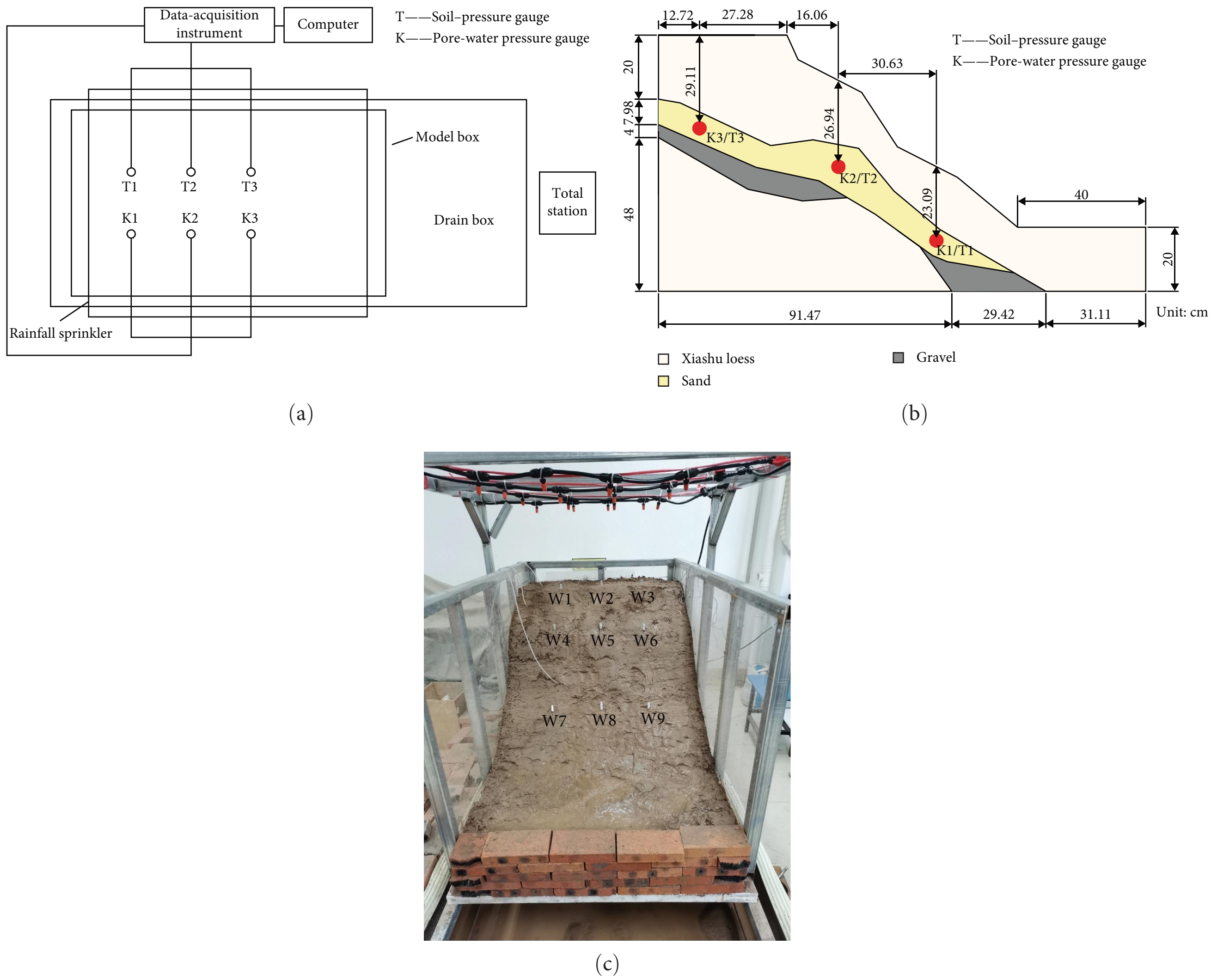

Figure 2: Model slope: (a) slope simulation device; (b) sensor location (the profile of slope model); and (c) deformation monitoring location.

model box to reduce the influence of the boundary effect and the friction between the filling material and the acrylic plate. Waterproof glue is used at the connection between the acrylic board and wood board to avoid rainwater seeping from the gap of the model box. The model box is placed on the reservoir to facilitate drainage and sediment deposition.

(2) After drying and crushing, the Xiashu loess was passed through a 2-mm sieve for subsequent model tests. The moisture content was set to 12%. To ensure the uniform distribution of water in the soil sample, the soil sample is not more than 50 kg each time. After repeated stirring, the soil samples were put into bags and stored for 48 hr. After the moisture content test results were qualified, the layered filling of the slope model was carried out. To ensure that the compaction degree of each filling is consistent, the slope soil is divided into eight layers, and the height of each layer is 10 cm after compaction. After the compaction of each layer, the soil samples of the middle and both sides were taken by the ring knife with a diameter of 61.8 mm and a height of 20 mm, and the compaction degree and water content were tested. The holes left by the ring knife sampling should be refilled and compacted to the original state. Before filling the next layer of soil, it is necessary to use a soil cutter to roughen the surface of the filled soil to make the two layers of soil tightly bonded. To avoid water loss and make the soil particles in the slope cemented with each other and the stress state tends to be stable, the surface of the slope model is covered with a plastic wrap. The test can be started after standing for 1 week.

(3) In order to ensure the accuracy of monitoring data, the sensor needs to be checked before installation. The pore-water pressure gauge needs to be saturated in water in advance, the air is discharged and then sealed immediately. To reduce the contact between the probe and the air, the sealing bag can be removed after the pore-water pressure gauge is buried in the soil. After the sensor is embedded, the soil is slightly compacted to ensure that the sensor is fixed and in full contact with the soil.

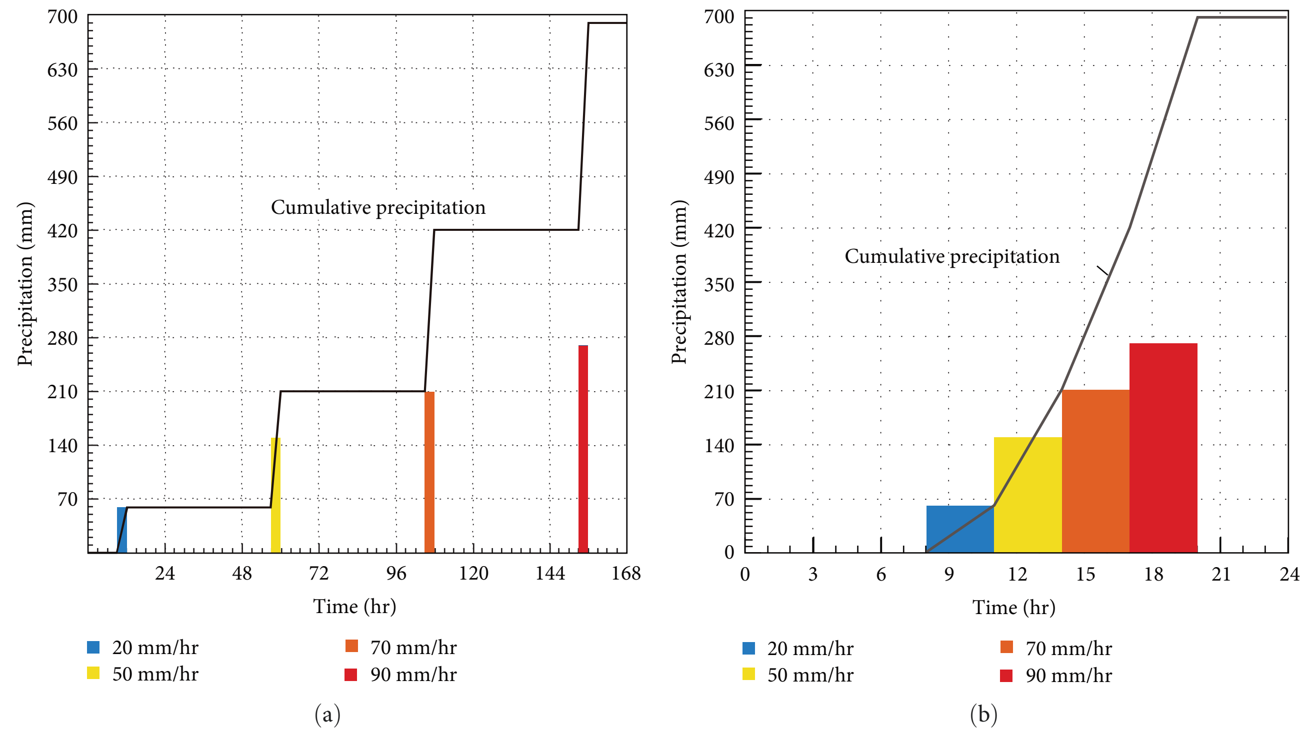

Figure 3: Rainfall plan: (a) intermittent rainfall; (b) persistent rainfall.

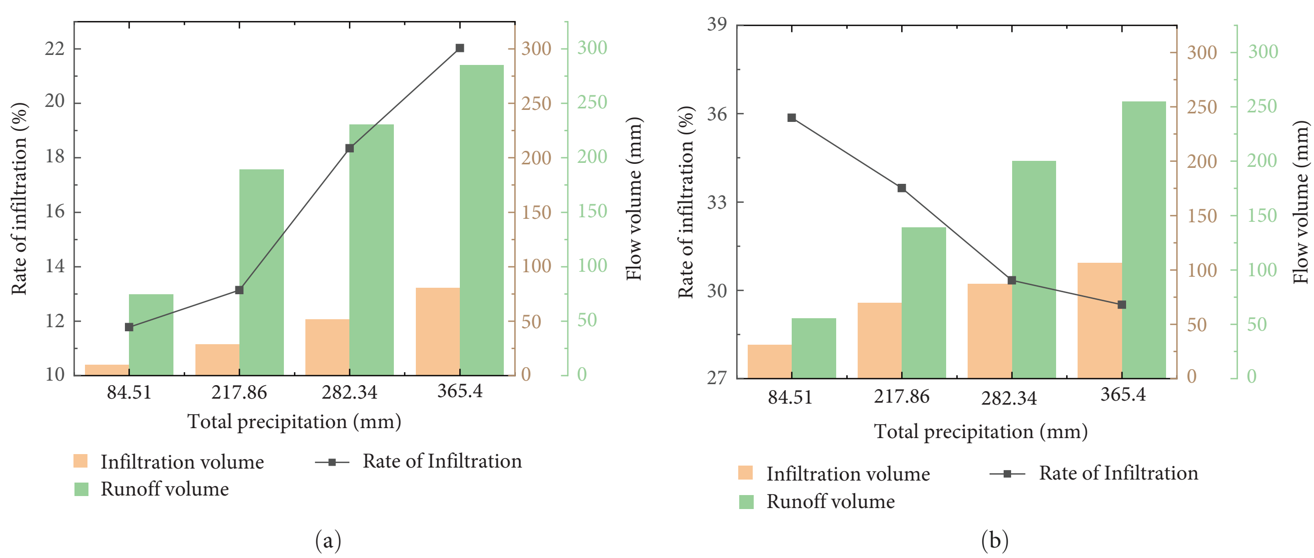

Figure 4: The infiltration of the soil slope under different rainfall conditions: (a) intermittent rainfall; (b) persistent rainfall.

(4) When filling the soil layer, where the deformation monitoring point is located, the prepared soil samples are evenly distributed in the layer, and the soil layer is compacted after inserting the monitoring support. It can effectively avoid the disturbance of the original stress field of the slope caused by the monitoring support. Select the appropriate position to set up the total station to ensure that it can receive the light reflected by the reflector of each monitoring point, to measure the displacement data of each point.

3. Results and Analysis

3.1. Law of Slope Runoff Infiltration. During the test, the total rainfall was monitored by the flowmeter. The runoff is calculated by measuring the water level change height of the reservoir. The results are shown in Figure 4.

The rainfall intensity set by the test is large. The permeability of Xiashu loess is weak, and rainwater is difficult to infiltrate. Surface runoff is generated quickly after rainfall. This shows that the rainfall intensity is greater than the infiltration capacity of Xiashu loess. Under the condition of intermittent rainfall, the infiltration rate of the first rainfall was only 11.78%. In the second rainfall, because the rainfall intensity was already greater than the infiltration rate, the infiltration rate did not increase significantly with the increase in rainfall intensity. At the beginning of the second rainfall, cracks appeared on the surface of the slope. Although the scale is small, it also plays a certain role in the increase of rainfall infiltration rate. During the third and fourth rainfall, the slope was moistened and dried, and the fissures were further developed and expanded. The rainfall infiltration rate increased significantly.

Because of the long-standing time, there are many cracks in the slope under the condition of continuous rainfall. The rainfall infiltration capacity of the slope is enhanced. The infiltration rate reached a maximum of 35.86% at the first continuous rainfall. After that, although the rainfall intensity increases, the rainfall infiltration rate gradually decreases. The analysis shows that in the early stage of rainfall, the soil moisture content on the slope surface is low, the crack opening degree is large, the rainwater infiltration is fast, and the infiltration rate is high. As the rainfall continues, the water content of the surface soil increases, and it begins to change from an unsaturated state to a saturated state. The matric suction decreases, the water content gradient decreases, and the rainfall infiltration capacity decreases. In addition, the Xiashu loess used in the test has weak expansibility. The soil absorbs water and expands, and the cracks become narrower, so the rainfall infiltration rate gradually decreases. However, the decrease of infiltration rate is small, indicating that the cracks are not completely closed. The soil structure has changed and the generation of the cracks is irreversible.

3.2. Variation Characteristics of Pore-Water Pressure. Based on the test data, the pore-water pressure of each monitoring point can be calculated. Figure 5 is the variation curve of pore-water pressure during intermittent rainfall. The initial values of pore-water pressure at the three monitoring points are similar, which are −1.30, −1.34, and−1.36 kPa, respectively. This is because the water content of the soil in each part of the slope is the same under the initial conditions, and there is no influence of diving. The rainfall intensity selected in the experiment was large, and the rainfall was much larger than the infiltration rate of rainwater, which soon formed slope runoff. The rainwater is collected to the foot of the slope, and the soil at the foot of the slope is infiltrated to form a transient saturated zone. As the rainfall progresses, the transient saturation zone moves downward. Rainwater first infiltrated into the K1 pore-water pressure gauge, causing changes in pore-water pressure. Due to the poor permeability of Xiashu loess, rainwater is difficult to infiltrate, so the change of pore-water pressure is small. The pore-water pressure did not change significantly for a long time after the beginning of rainfall. After about 50 min, the pore-water pressure of K1 began to increase first. K2 and K3 are relatively far from the slope, and it takes a longer time for pore-water pressure to change significantly.

During the first rainfall, rainwater accumulated at the top of the slope. When the rainfall stops, the water on the top of the slope continues to infiltrate. The water on the slope moves downward under the action of gravity. Therefore, the pore-water pressure of the three points even increased slightly for a period after the rainfall stopped and then began to decline slowly. This phenomenon indicates that the change in pore-water pressure has hysteresis. Since then, with the increase in standing time, although the decrease of pore-water pressure can be observed, the decrease is small. The position of the slope toe is lower, and the most infiltration recharge is received, so the pore-water pressure of the monitoring point K1 is the largest, which is −0.95 kPa. The pore-water pressure of monitoring point K2 and K3 is −1.13 and −1.28 kPa, respectively.

Due to the poor permeability of Xiashu loess, it is difficult to drain the infiltration rainwater along the foot of the slope. To a certain extent, it limits the reduction of pore-water pressure. Therefore, the initial value of pore-water pressure during the second rainfall is greater than that during the first rainfall. Because of the appearance of cracks, the rainfall infiltration increases, and the pore-water pressure changes obviously. The maximum pore-water pressure at K1 increased by 52.87%, which was 1.94 times that of the first rainfall. Compared with the first rainfall, the pore-water pressure curve of this stage has some slight fluctuations.

At the third rainfall, the soil at K1 began to transition from an unsaturated state to a saturated state. The value of pore-water pressure begins to change from negative to positive at about the end of rainfall. During the fourth rainfall, the pore-water pressure fluctuates up and down due to a small range of soil collapse in this stage. Due to the small failure range and shallow failure depth of the soil, the overall trend of pore-water pressure has not been significantly affected. At the end of rainfall, the pore-water pressure of K1, K2, and K3 was 0.92, 0.27, and 0.45 kPa, respectively.

The variation of pore-water pressure under continuous rainfall conditions is shown in Figure 6. Compared with intermittent rainfall, pore-water pressure changes faster and fluctuates more. This is because the slope has repeatedly undergone rainwater infiltration softening and standing, and there are many cracks on the surface. About 3 hr after the rainfall began, the landslide caused the sand layer to emerge, and the groundwater in the slope was excreted and lost from this part. The rainwater infiltration is too late to recharge the place, and the pore-water pressure drops suddenly and fluctuates continuously. It can be seen from the trend of the three curves that the pore-water pressure of the K1 at the foot of the slope changes most sharply before and after the slope failure, and the difference can reach 0.47 kPa. K2 and K3 were relatively less affected.

After a period, the soil on the free surface continues to collapse under rainfall erosion. The scattered soil covers the exposed sand, and the pore-water pressure begins to rise gradually. The growth rate of pore-water pressure began to slow down after about 7 hr of rainfall. After 8 hr, the pore-water pressure at K1 no longer increases significantly. Shortly after that, the change of pore-water pressure at K2

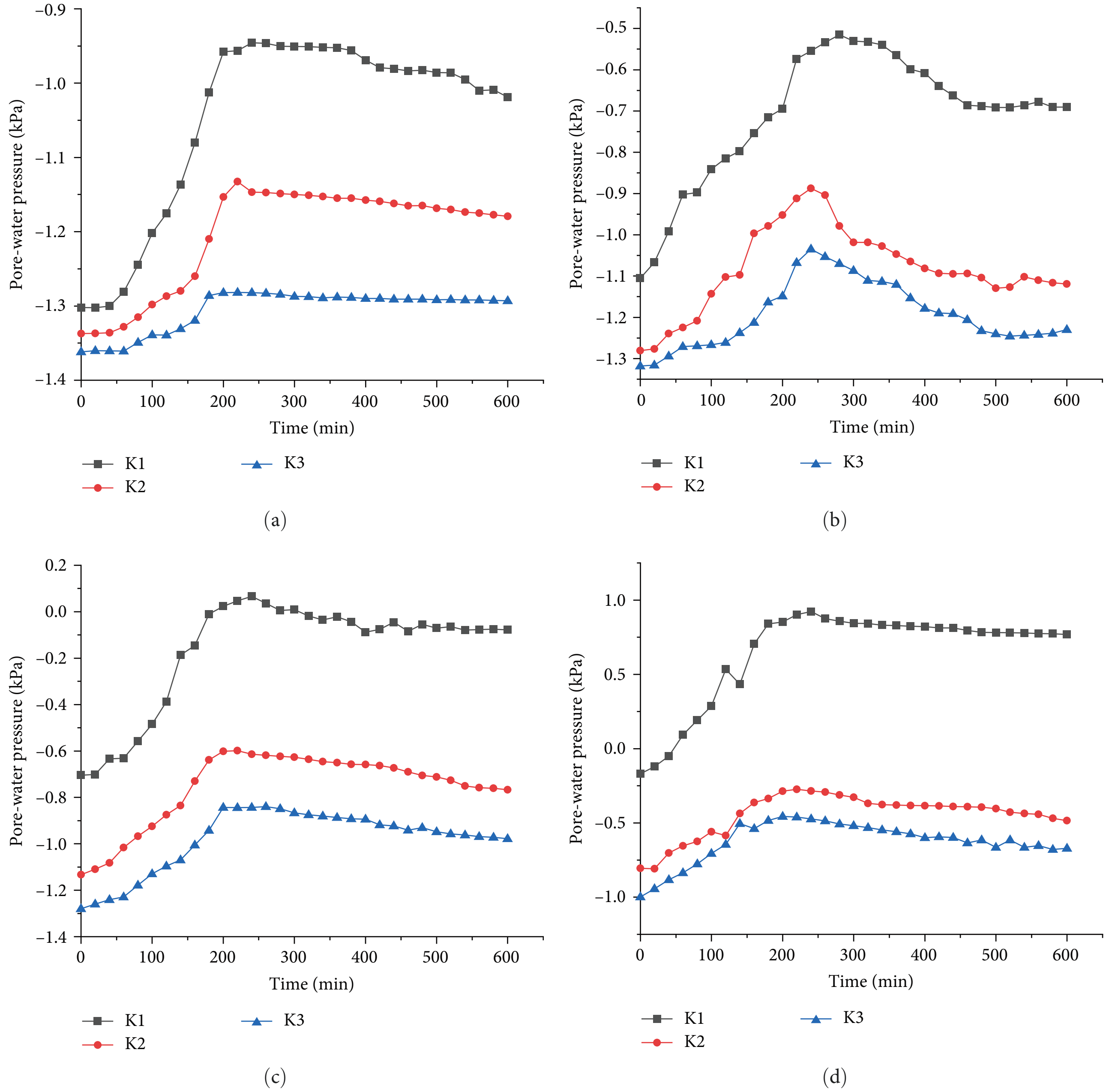

Figure 5: Pore-water pressure curve of intermittent rainfall: (a) the first rainfall, (b) the second rainfall, (c) the third rainfall, and (d) the fourth rainfall.

and K3 monitoring points also tended to be gentle. This indicates that the slope is saturated and begins to drain outward. After the rainfall stopped, the pore-water pressure did not decrease immediately, and it showed a downward trend after about 30 min.

3.3. Variation Characteristics of Vertical Stress. The variation curve of vertical stress under intermittent rainfall is shown in Figure 7. The initial vertical stress of the three monitoring points is related to the depth of the sensor. The T1 monitoring point is located at the foot of the slope, with the shallowest buried depth and the smallest vertical stress of 4.16 kPa. The monitoring points of T2 and T3 are located at the top and middle of the slope, and the vertical stress is 4.73 and 5.88 kPa, respectively.

At the beginning of the first rainfall, the vertical stress did not change immediately because the rainwater washed away the loose soil on the slope surface and the infiltration was slow. It began to rise slowly after a period. The trend of the three vertical stress change curves is roughly the same. In the early stage of rainfall, rainwater infiltration is relatively fast, the weight of soil in the infiltration area increases, and the vertical stress increases rapidly. After a period, the surface soil of the slope is saturated, the rainwater infiltration rate decreases, and the vertical stress increases slowly. After the rainfall stopped, the vertical stress did not decrease

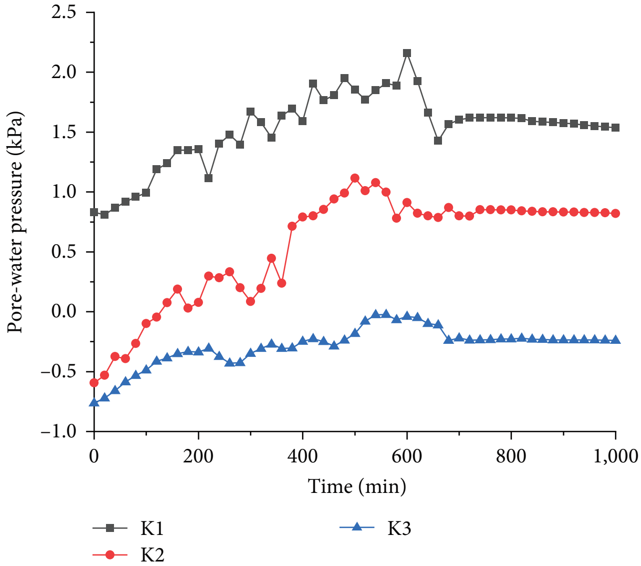

Figure 6: Pore-water pressure curve of continuous rainfall.

immediately because the rainwater accumulated at the top of the slope continued to infiltrate. Shortly after the water on the top of the slope disappeared, the vertical stress of the T2 and T3 monitoring points began to decrease. The T1 monitoring point is located at the foot of the slope and can still receive infiltration recharge, so the reduction of the vertical stress is relatively lagging.

In the second rainfall, the changing trend of vertical stress is like that of the first rainfall, but the increment is relatively large. About 20 min after the end of rainfall, the vertical stress of the T1 monitoring point increased from 4.60 to 5.48 kPa. The maximum vertical stress of the T2 monitoring point is 5.49 kPa. After the rainfall stops, the vertical stress decreases. About 100 min after the end of the rainfall, the vertical stress of the T2 monitoring point is smaller than that of the T1 monitoring point. The increment of vertical stress at the T3 monitoring point is the smallest, only 0.50 kPa.

At the third rainfall, although the rainfall infiltration increased, the groundwater level in the sand layer continued to rise due to the saturation of the slope toe. This leads to the growth rate of vertical stress at the T1 point being much smaller than that at the other two monitoring points under the uplift pressure generated by the temporary confined water formed by the gravel layer. At the beginning of rainfall, the vertical stress of the T1 monitoring point is 5.23 kPa. The maximum value of 5.64 kPa was reached at about 240 min after the beginning of rainfall. The initial vertical stress of T2 and T3 monitoring points is 5.21 and 6.35 kPa. The maximum values were 5.91 and 7.20 kPa, respectively, at about 40 and 20 min after the end of rainfall.

At the fourth rainfall, the vertical stress at T2 and T3 points continued to increase as the rainfall continued. The maximum values are 5.93 and 7.26 kPa. The vertical stress at point T1 almost did not change significantly at the beginning of rainfall, and even slightly decreased. The vertical stress before slope failure was 5.42 kPa. Because the upper and lower parts of the sand layer and the gravel layer are weakly permeable to slightly permeable Xiashu loess, the stratum will produce temporary confined water. Coupled with the rising water level, the pore-water pressure increases, so the vertical stress at the monitoring point decreases. Soil collapse occurred about 2 hr after the beginning of rainfall, and the vertical stress of the three monitoring points suddenly decreased. Because T1 was the closest to each other, it was most affected.

The variation curve of vertical stress under continuous rainfall is shown in Figure 8. The trend of vertical stress change at T1, T2, and T3 is roughly the same. In the early stage of rainfall, rainwater infiltration increases the water content of the soil, the bulk density of the soil increases, and the vertical stress increases rapidly. About 200 min after the rainfall, the soil loss and crack development led to the collapse of the slope and the vertical stress decreased suddenly. The decrease at T3 is the largest, which is due to the gradual collapse of the slope at the top of the slope and the large loss of soil at the top of the slope. After collapse, the slope is in a temporary stable state, and the vertical stress tends to be stable. With the infiltration and erosion of rainwater, the cracks continue to develop into the deep part of the slope, the soil collapses again, and the vertical stress suddenly decreases. The slope is stable after the soil collapses and the crack development causes the soil to collapse again, so the vertical stress shows two states of the sudden decline and stabilization. After the rainfall is stopped, due to the small permeability coefficient of Xiashu soil, the water in the slope is difficult to discharge, and the vertical pressure decreases slowly.

3.4. Slope Deformation Failure Process and Mechanism Analysis. The deformation and failure process of the slope can be divided into the slope surface erosion deformation stage, the local failure stage of the slope, the failure stage of the leading edge of the slope, and the large-scale failure stage in the middle of the slope.

3.4.1. Slope Failure under Intermittent Rainfall. Figure 9 is the deformation and failure diagram of the slope during intermittent rainfall. At the beginning of the first rainfall, the slope soil was exposed and directly impacted by the raindrops. The loose soil particles on the surface migrated and blocked the pores in the soil. This leads to a decrease in rainwater infiltration capacity, and excess rainwater converges on the slope to form surface runoff. At this time, the rainfall intensity is relatively small, and the erosion of runoff on the slope is limited, mainly manifested as splash erosion and sheet erosion. With the continuous erosion of rainwater, the erosion effect gradually increases, and small erosion ditches begin to form locally. At the end of the rainfall, the small erosion ditches are interconnected to form two obvious erosion ditches. They are roughly distributed in parallel along the slope. One is longer, extending from the top of the slope to the foot of the slope, and the other is shorter, extending only from the top of the slope to the middle and lower part of the slope.

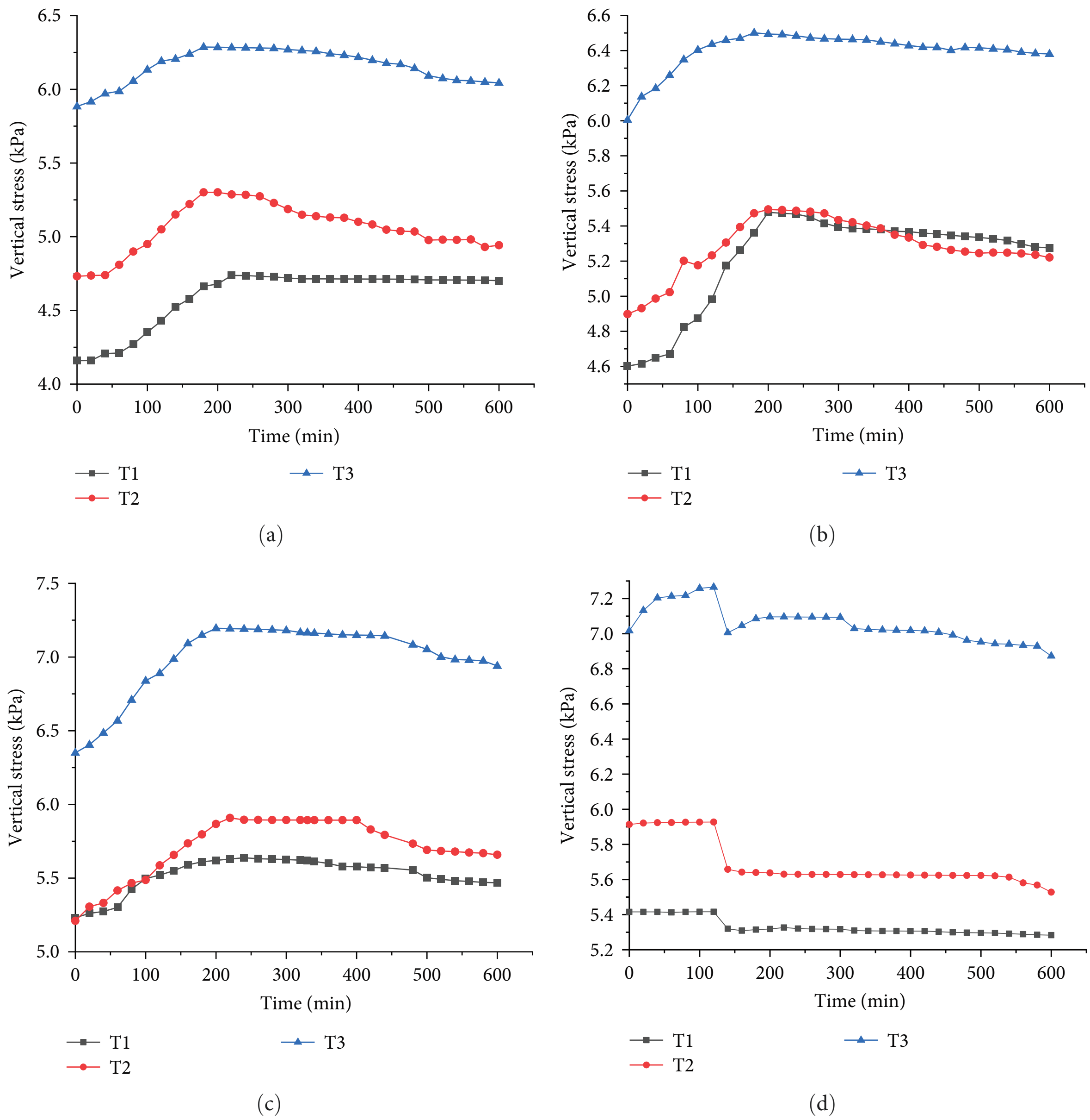

FIGURE 7: Vertical stress variation curve of intermittent rainfall: (a) the first rainfall, (b) the second rainfall, (c) the third rainfall, and (d) the fourth rainfall.

The second rainfall intensity was significantly enhanced, the potential energy of raindrop landing was greater, and the scouring effect was stronger. Part of the rainwater converges in the erosion groove and flows to the foot of the slope. The surrounding soil begins to crack due to immersion softening, and the erosion gradually develops to both sides and inside the slope.

In the third rainfall, the slope developed more cracks, and the rainwater was more permeable. The amount of rainfall entering the gravel layer increases, the soil weight increases, and some sand particles move downward with the rain into the gap between the gravels. Some positions began to appear as hollow areas. Because the permeability of the gravel layer is much larger than that of the underlying Xiashu loess layer, the rainwater is not easy to infiltrate. It converges in this layer, causing the rise of groundwater level.

At the fourth rainfall, the two gullies continued to expand and eventually converged. The intermediate soil is cut to form a free surface. Due to the softening of rainwater infiltration, the soil weight becomes larger, and the sliding force increases. According to the indoor test results, with the increase of water content, the strength of Xiashu loess will decay rapidly, resulting in the decrease of antisliding force and the collapse of some soil. The collapsed soil is relatively soft, and it continues to move to the toe of the slope under the erosion of runoff. The newly formed free surface is further expanded.

During the whole intermittent rainfall process, only monitoring points W1 and W4 are greatly affected by the landslides. Because only the surface soil collapses, and the monitoring support is buried deeper, the displacement of

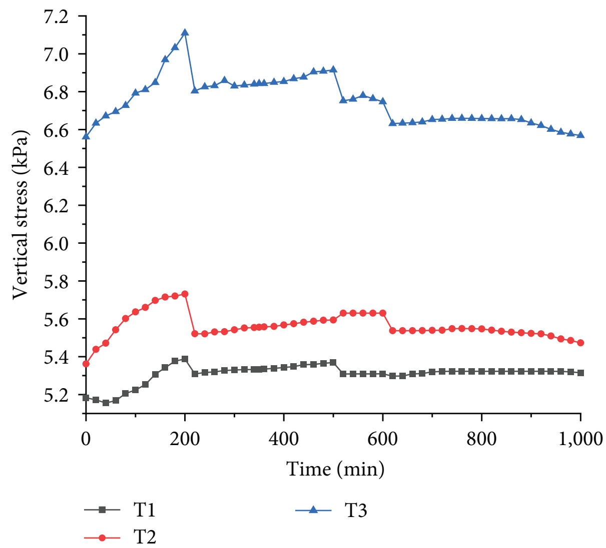

Figure 8: Vertical stress variation curve of continuous rainfall.

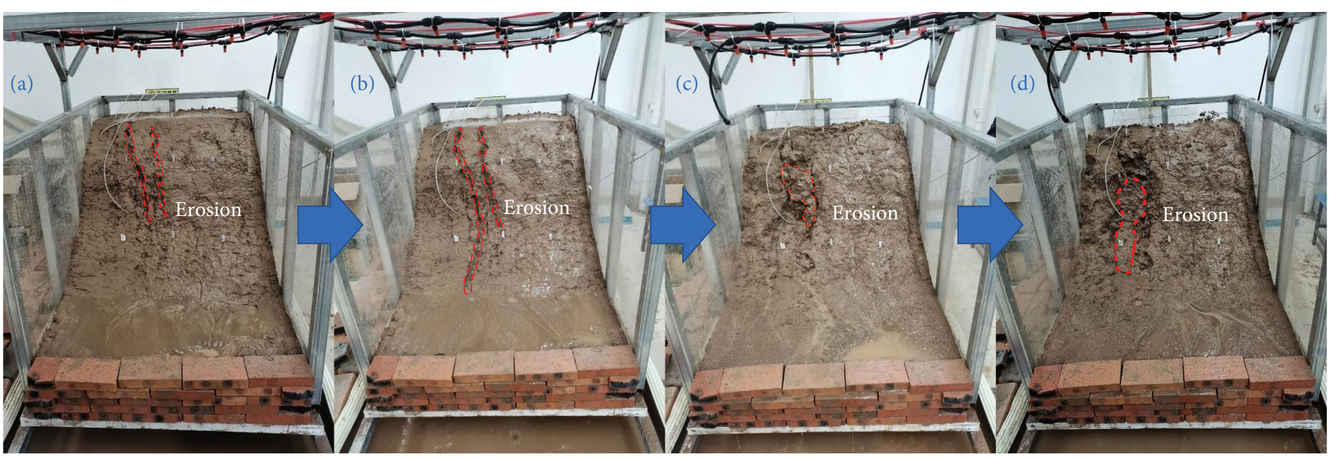

Figure 9: Schematic diagram of slope failure process during intermittent rainfall: (a) the first rainfall, (b) the second rainfall, (c) the third rainfall, and (d) the fourth rainfall.

these two points is smaller. No obvious displacement occurred at other monitoring points. In the early stage of rainfall, the failure of the slope model is only manifested as the gully formed by rainfall erosion. Currently, the gully is shallow and has little effect on the displacement of the deeper soil, so only the monitoring points W1–W4 produce a small displacement. In the later stage of rainfall, the soil around monitoring point W4 collapsed, and the point produced a large displacement. The vertical displacement is 1.46 cm, and the horizontal displacement is relatively small, only 0.22 cm. The monitoring stent was obviously exposed. W1–W3 monitoring points are located at the top of the slope, and the downward settlement displacement can be monitored. The value is small, indicating that the creep settlement occurs at the top of the slope.

3.4.2. Slope Failure under Continuous Rainfall. After the intermittent rainfall, the slope model experienced 4 days of standing. Xiashu loess produces many cracks due to water loss shrinkage. After the start of continuous rainfall, due to the loss of support at the free surface of the soil, small soil blocks continue to fall. The deformation and failure of the slope during continuous rainfall are shown in Figure 10. Rainwater infiltration increased significantly with the duration of rainfall. The water level in the gravel layer rises obviously, infiltrating the contact surface between loess soil and sand, softening it and reducing its strength.

The upper soil increased heavily due to rainfall infiltration. Coupled with the infiltration softening and floating effect of rainwater, the sliding force of the soil increases and the shear strength decreases. The continuous development and expansion of tensile cracks in the soil provide a way for the rapid infiltration of rainwater. Rainwater accumulates in the cracks and infiltrates into the surrounding soil to form a transient saturated zone. As the crack expands, the transient saturated zone expands. When the crack penetrates, landslides begin to appear. Due to the dynamic effect of the landslide, new cracks are generated. The original crack

Figure 10: Schematic diagram of slope failure process during continuous rainfall: (a) 3 hr rainfall and (b) 8 hr rainfall.

Figure 11: Fracture development: (a) cracks on the top of the slope and (b) the transverse cracks below the slope.

opening degree becomes larger, making the sliding body lose and increasing rainfall infiltration. Due to the sliding of the lower soil, the slope has a free surface, which makes the upper soil lose support and deform, which is a typical traction landslide.

During the continuous rainfall process, the monitoring point W4 support leans forward, and the soil displacement at this point continues to change. The monitoring point W5 also began to show displacement changes because the failure zone expanded to the surrounding area. The monitoring points W6–W7 are less affected because of the long distance, and there is no significant displacement change. At the end of the rainfall, the displacement of the monitoring point W4 was the largest, the vertical displacement was 5.83 cm, and the horizontal displacement was 3.67 cm. The monitoring point W2 has the largest settlement of 3.11 cm.

By analyzing the displacement changes of monitoring points at different positions, the slope top first generates displacement, and the slope surface is relatively late. This is because rainwater has a downward infiltration force in the slope, while water infiltration rate is faster at the top of the slope and slower on the slope. When the slope appears transient saturation, the tensile stress decreases, and the slope soil appears tensile cracks. It began to show a trend of forward movement, aggravating the increase of horizontal displacement. Figure 11(a) shows the cracks appearing at the top of the slope, which are small in width and gradually developed in the later stage. Figure 11(b) is a transverse fissure below the slope, about 10 cm in length.

4. Conclusion

Through the artificial rainfall test of the soil slope model with a sandy gravel layer, the slope deformation, pore-water pressure, and vertical stress change were observed in real-time, and the relevant variation law of the slope under the condition of rainwater infiltration was obtained. The slope instability mechanism under different rainfall conditions was analyzed. The conclusions are as follows:

(1) The difference in the influence of different rainfall types on the slope is mainly due to the difference in rainfall infiltration capacity. The rainfall infiltration rate of intermittent rainfall increased with the increase of rainfall times, from 11.78% in the first time to 22.03% in the fourth time. The rainfall infiltration rate of continuous rainfall decreased with the rainfall process, and the highest was 35.86%.

(2) The increase of pore-water pressure after different rainfall types is the largest at the foot of the slope. In intermittent rainfall, the vertical pressure growth rates of the three monitoring points are similar. In continuous rainfall, the vertical pressure curve is steep, and the slope top changes the most.

(3) The instability mechanism of Xiashu loess slope with gravel layer under rainfall conditions is as follows: rainwater infiltration and soaking softening soil lead to fracture development, a decrease of shear strength, and small-scale damage of slope. The water level of the gravel layer rises to form a temporary confined water layer, which produces uplift pressure on the upper soil. The pore-water pressure increases and the soil fissures further expand and penetrate, resulting in the collapse of the free surface soil.

Data Availability

The data used to support the findings of this study are available from the corresponding author upon request.

Conflicts of Interest

The authors declare that they have no conflicts of interest.

Authors' Contributions

Yanran Hu performed data curation and formal analysis, validated the study, and wrote the original draft. Shaorui Sun conceptualized the study, proposed the methodology, supervised the study, revised the original draft, and performed funding acquisition. Yuyong Sun performed data curation and formal analysis and revised the original draft. All authors have read and agreed to the published version of the study and agreed to be accountable for all aspects of the work.

Acknowledgments

The research is funded by Natural Science Foundation of China (No. 42007256 and 41672258), and the Natural Key projects in Anhui Province (2022AH051751, KJ2021ZD0125, 2022AH051748).

References

[1] A. M. Han, H. Li, and H. Z. Xu, "Hydro mechanical behaviour of Nanjing Xiashu loess in desorption moisture state," *Journal of Engineering Geology*, vol. 24, no. 2, pp. 268–275, 2016.

[2] S. Sun, W. Wang, J. Wei et al., "The physical–mechanical properties degradation mechanism and microstructure response of acid–alkali-contaminated Xiashu loess," *Natural Hazards*, vol. 106, no. 3, pp. 2845–2861, 2021.

[3] S. Liu, Y. Wang, G. Cai, P. Jiang, J. Wang, and M. Zhang, "Experimental study on the effects of wet-dry cycles and suction on the mechanical properties of unsaturated Xiashu loess," *Journal of Southeast University (Natural Science Edition)*, vol. 51, no. 3, pp. 473–479, 2021.

[4] W. Wang, S. Liu, Z. Yang, and L. Wu, "Study on deformation characteristics of Xiashu loess in Zhenjiang under dry-wet cycles," *South China Journal of Seismology*, vol. 41, no. 2, pp. 99–104, 2021.

[5] Y. Hu, S. Sun, and J. Wei, "Effect of cementation degree on shear characteristic and failure mechanism of bimrocks containing gravels of different sizes," *Lithosphere*, vol. 2022, no. Special 10, Article ID 1334579, 2022.

[6] Y. Hu, S. Sun, and K. Li, "Study on influence of moisture content on strength and brittle–plastic failure characteristics of Xiashu loess," *Advances in Civil Engineering*, vol. 2023, Article ID 5919325, 10 pages, 2023.

[7] S. Liu, G. Cai, and T. Cheng, "Stability analysis of Xiashu loess slope under rainfall infiltration," *Journal of Geological Hazards and Environment Preservation*, vol. 33, no. 2, pp. 32–37, 2022.

[8] W. Ye and Y. Zhang, "Model test study on instability of loess slopes under long-term rainfall," *China Sciencepaper*, vol. 16, no. 6, pp. 603–609, 2021.

[9] J. Chong, X. Li, and D. Yang, "Slope geologic disasters in Zhenjiang city and countermeasures against them," *Journal of Catastrophology*, vol. 17, no. 1, pp. 20–26, 2002.

[10] W.-C. Wang, S.-R. Sun, J.-H. Wei, Y.-X. Yu, W. He, and J.-L. Song, "Numerical experimental study on optimum design of anchorage system for Xiashu loess slope," *Journal of Central South University*, vol. 28, no. 9, pp. 2843–2856, 2021.

[11] J. Qu, Y. Lu, S. Wu, J. Liu, and F. Gou, "Evaluation of Xiashu loess slope stability in Zhenjiang area using different methods," *The Chinese Journal of Geological Hazard and Control*, vol. 32, no. 1, pp. 35–42, 2021.

[12] J.-S. Zhao, Q. Jiang, J.-F. Lu, B.-R. Chen, S.-F. Pei, and Z.-L. Wang, "Rock fracturing observation based on microseismic monitoring and borehole imaging: in situ investigation in a large underground cavern under high geostress," *Tunnelling and Underground Space Technology*, vol. 126, Article ID 104549, 2022.

[13] J.-S. Zhao, Q. Jiang, S.-F. Pei, B.-R. Chen, D.-P. Xu, and L.-B. Song, "Microseismicity and focal mechanism of blasting-induced block falling of intersecting chamber of large underground cavern under high geostress," *Journal of Central South University*, vol. 30, no. 2, pp. 542–554, 2023.

[14] Y. Okura, H. Kitahara, H. Ochiai, T. Sammori, and A. Kawanami, "Landslide fluidization process by flume

experiments," *Engineering Geology*, vol. 66, no. 1-2, pp. 65–78, 2002.

[15] H. Rahardjo, T. T. Lee, E. C. Leong, and R. B. Rezaur, "Response of a residual soil slope to rainfall," *Canadian Geotechnical Journal*, vol. 42, no. 2, pp. 340–351, 2005.

[16] E. Damiano and L. Olivares, "The role of infiltration processes in steep slope stability of pyroclastic granular soils: laboratory and numerical investigation," *Natural Hazards*, vol. 52, no. 2, pp. 329–350, 2010.

[17] Z.-H. Guo, W.-B. Jian, Q.-L. Liu, and W. Nie, "Rainfall infiltration analysis and infiltration model of slope based on in-situ tests," *Rock and Soil Mechanics*, vol. 42, no. 6, pp. 1635–1647, 2021.

[18] S. Sun, K. Li, H. Le et al., "Study on the deterioration characteristics of greenschist under hydrochemical action and the disaster-causing mechanism in slope," *Bulletin of Engineering Geology and the Environment*, vol. 81, no. 8, pp. 315–341, 2022.

[19] R. Yu, Y. Xu, T. Zhou, and J. Li, "Relation between rainfall duration and diurnal variation in the warm season precipitation over central eastern China," *Geophysical Research Letters*, vol. 34, no. 13, pp. 3–7, 2007.

[20] A. Rosi, T. Peternel, M. Jemec-Auflič, M. Komac, S. Segoni, and N. Casagli, "Rainfall thresholds for rainfall-induced landslides in Slovenia," *Landslides*, vol. 13, no. 6, pp. 1571–1577, 2016.

[21] P. Sun, G. Wang, R. Li et al., "Study on field test of loess slope under the artificial rainfall condition," *Journal of Engineering Geology*, vol. 27, no. 2, pp. 466–476, 2019.

[22] T. Du, Z. Li, X. Wang et al., "Model experiment study on erosion of loess slope due to rainfall," *Journal of Engineering Geology*, vol. 26, no. 3, pp. 732–740, 2018.

[23] Z. Guo, Q. Huang, Y. Liu, Q. Wang, and Y. Chen, "Model experimental study on the failure mechanisms of a loess–bedrock fill slope induced by rainfall," *Engineering Geology*, vol. 313, Article ID 106979, 2023.

[24] Q. Fan, J. Liu, D. Yang, and J. Yuan, "Model test study of expansive rock slope under different types of precipitation," *Rock and Soil Mechanics*, vol. 37, no. 12, pp. 3401–3409, 2016.

[25] H. Hu, Z. P. Hu, and R. Ruan, "Research on landslide simulated experiment and slope sliding mesoscopic rule of granite residual soil under heavy rainfall," *Journal of Xiamen University (Natural Science)*, vol. 59, no. 4, pp. 583–589, 2020.

[26] C.-L. Zeng, R.-J. Li, X.-D. Guan, S.-B. Zhang, and W.-S. Bai, "Experimental study on rainfall infiltration characteristics of loess slopes under different rainfall intensities," *Chinese Journal of Geotechnical Engineering*, vol. 42, no. S1, pp. 111–115, 2020.

[27] H. Zhu, B. Shi, J. Yan et al., "Physical model testing of slope stability based on distributed fiber-optic strain sensing technology," *Chinese Journal of Rock Mechanics and Engineering*, vol. 32, no. 4, pp. 821–828, 2013.

[28] A. Chueasamat, T. Hori, H. Saito, T. Sato, and Y. Kohgo, "Experimental tests of slope failure due to rainfalls using 1g physical slope models," *Soils and Foundations*, vol. 58, no. 2, pp. 290–305, 2018.

[29] W. A. Take, M. D. Bolton, P. C. P. Wong, and F. J. Yeung, "Evaluation of landslide triggering mechanisms in model fill slopes," *Landslides*, vol. 1, no. 3, pp. 173–184, 2004.

[30] A. Tohari, M. Nishigaki, and M. Komatsu, "Laboratory rainfall-induced slope failure with moisture content measurement," *Journal of Geotechnical and Geoenvironmental Engineering*, vol. 133, no. 5, pp. 575–587, 2007.

[31] C. Gallage, T. Abeykoon, and T. Uchimura, "Instrumented model slopes to investigate the effects of slope inclination on rainfall-induced landslides," *Soils and Foundations*, vol. 61, no. 1, pp. 160–174, 2021.

[32] R. P. Orense, S. Shimoma, K. Maeda, and I. Towhata, "Instrumented model slope failure due to water seepage," *Journal of Natural Disaster Science*, vol. 26, no. 1, pp. 15–26, 2004.